New Journal of Physics
The open access journal at the forefront of physics

Deutsche Physikalische Gesellschaft DPG IOP Institute of Physics

FAST TRACK COMMUNICATION • OPEN ACCESS

Enhanced superconductivity due to forward scattering in FeSe thin films on $SrTiO_3$ substrates

New Journal of Physics
The open access journal at the forefront of physics

Deutsche Physikalische Gesellschaft DPG
IOP Institute of Physics

Published in partnership with: Deutsche Physikalische Gesellschaft and the Institute of Physics

OPEN ACCESS

RECEIVED
5 November 2015

REVISED
4 January 2016

ACCEPTED FOR PUBLICATION
26 January 2016

PUBLISHED
10 February 2016

FAST TRACK COMMUNICATION

Enhanced superconductivity due to forward scattering in FeSe thin films on $SrTiO_3$ substrates

Louk Rademaker[1], **Yan Wang**[2], **Tom Berlijn**[3,4] **and Steve Johnston**[2,5]

[1] Kavli Institute for Theoretical Physics, University of California Santa Barbara, CA 93106, USA
[2] Department of Physics and Astronomy, University of Tennessee, Knoxville, TN 37996, USA
[3] Center for Nanophase Materials Sciences, Oak Ridge National Laboratory, Oak Ridge, TN 37831, USA
[4] Computer Science and Mathematics Division, Oak Ridge National Laboratory, Oak Ridge, TN 37831, USA
[5] Author to whom any correspondence should be addressed.

E-mail: sjohn145@utk.edu

Keywords: superconductivity, electron-phonon interactions, Eliashberg theory, FeSe thin films

Supplementary material for this article is available online

Communicated by NJP Board member Peter Hirschfeld

Abstract

We study the consequences of an electron–phonon (e–ph) interaction that is strongly peaked in the forward scattering ($\mathbf{q} = 0$) direction in a two-dimensional superconductor using Migdal–Eliashberg theory. We find that strong forward scattering results in an enhanced T_c that is linearly proportional to the strength of the dimensionless e–ph coupling constant λ_m in the weak coupling limit. This interaction also produces distinct replica bands in the single-particle spectral function, similar to those observed in recent angle-resolved photoemission experiments on FeSe monolayers on $SrTiO_3$ and $BaTiO_3$ substrates. By comparing our model to photoemission experiments, we infer an e–ph coupling strength that can provide a significant portion of the observed high T_c in these systems.

A flurry of scientific activities has been generated by the discovery of an enhanced superconductivity in FeSe monolayers grown on $SrTiO_3$ (STO) substrates [1–20]. On its own, bulk FeSe has a modest superconducting transition temperature $T_c \sim 9$ K [21]; however, when a monolayer is grown on an STO substrate, T_c is increased dramatically [1]. Most reported T_c values cluster within 55–75 K, close to the boiling point of liquid nitrogen (77 K). (A surprisingly high $T_c \sim 107$ K has also been reported in *in situ* transport measurements [9].) This discovery has opened a pathway to high-T_c superconductivity through interface engineering, which has already produced high-T_c's in systems such as FeSe on $BaTiO_3$ (BTO) [8] and $FeTe_{1-x}Se_x$ on STO [22].

Determining the origin of the T_c enhancement in these interface systems is critical. At the moment, proposals include charge transfer between the substrate and FeSe [2–4, 20], electric field [6] and strain effects due to the substrate [5, 8], and lattice related effects such as enhanced electron–phonon (e–ph) coupling in the FeSe layer [1, 13, 16] or across the interface [7, 19]. Strong evidence for the latter has been provided by a recent angle-resolved photoemission spectroscopy (ARPES) study [7], which observed replica bands in the single-particle spectral function of the FeSe monolayer. These replicas are interpreted as being produced by coupling between the FeSe 3*d* electrons and an optical oxygen phonon branch in the STO substrate. Moreover, the replica bands are complete copies of the corresponding main bands, which implies that the responsible e–ph interaction is strongly peaked in the forward scattering direction (small momentum transfers). Such momentum dependence is notable because it can enhance superconductivity in most pairing channels [23–31]. As such, this cross-interface coupling provides at the same time a suitable mechanism for the T_c enhancement in the FeSe/STO and FeSe/BTO systems [7, 8].

We explore this possibility here by examining the consequences of strong forward scattering in the e–ph interaction for superconductivity and the spectral properties of a two-dimensional system. By solving the momentum dependent Eliashberg equations, we show that a pronounced forward scattering results in a T_c that

scales linearly with the dimensionless e–ph coupling constant λ_m (see below) in the weak coupling limit. This is in stark contrast to the usual exponential dependence predicted by BCS theory. Furthermore, this coupling produces distinct replica structures in the spectral function similar to those observed experimentally. By comparing our model to experiments [7], we infer a significant e–ph contribution to the total T_c observed in the FeSe/STO system with a modest value of λ_m.

1. Formalism

To model the FeSe monolayer we consider a single-band model for the FeSe electron pockets, which includes coupling to an oxygen phonon branch in the STO substrate. The Hamiltonian is given by

$$H = \sum_{\mathbf{k},\sigma} \xi_{\mathbf{k}} c^{\dagger}_{\mathbf{k},\sigma} c_{\mathbf{k},\sigma} + \sum_{\mathbf{q}} \Omega_{\mathbf{q}} b^{\dagger}_{\mathbf{q}} b_{\mathbf{q}} + \frac{1}{\sqrt{N}} \sum_{\mathbf{k},\mathbf{q},\sigma} g(\mathbf{k}, \mathbf{q}) c^{\dagger}_{\mathbf{k}+\mathbf{q},\sigma} c_{\mathbf{k},\sigma} (b^{\dagger}_{-\mathbf{q}} + b_{\mathbf{q}}),$$

where $c^{\dagger}_{\mathbf{k},\sigma}$ ($c_{\mathbf{k},\sigma}$) and $b^{\dagger}_{\mathbf{q}}$ ($b_{\mathbf{q}}$) are electron and phonon creation (annihilation) operators, respectively, $\xi_{\mathbf{k}}$ is the band dispersion, $\Omega_{\mathbf{q}}$ is the phonon dispersion, and $g(\mathbf{k}, \mathbf{q})$ is the momentum-dependent e–ph coupling constant.

We calculate the single-particle self-energy due to the e–ph interaction using Migdal–Eliashberg theory. Using the Nambu notation with fermionic Matsubara frequencies $\omega_n = (2n + 1)\pi/\beta$, where $\beta = 1/T$ is the inverse temperature, the self-energy is $\hat{\Sigma}(\mathbf{k}, i\omega_n) = i\omega_n[1 - Z(\mathbf{k}, i\omega_n)]\hat{\tau}_0 + \chi(\mathbf{k}, i\omega_n)\hat{\tau}_3 + \phi(\mathbf{k}, i\omega_n)\hat{\tau}_1$, where $\hat{\tau}_i$ are the Pauli matrices, $Z(\mathbf{k}, i\omega_n)$ and $\chi(\mathbf{k}, i\omega_n)$ renormalize the single-particle mass and band dispersion, respectively, and $\phi(\mathbf{k}, i\omega_n)$ is the anomalous self-energy, which is zero in the normal state. The self-energy is then computed by self-consistently evaluating the one-loop diagram and is given by

$$\hat{\Sigma}(\mathbf{k}, i\omega_n) = \frac{-1}{N\beta} \sum_{\mathbf{q},m} |g(\mathbf{k}, \mathbf{q})|^2 D^{(0)}(\mathbf{q}, i\omega_n - i\omega_m)\hat{\tau}_3 \hat{G}(\mathbf{k} + \mathbf{q}, i\omega_m)\hat{\tau}_3,$$

where $D^{(0)}(\mathbf{q}, i\omega_\nu) = -\frac{2\Omega_{\mathbf{q}}}{\Omega^2_{\mathbf{q}} + \omega^2_\nu}$ is the bare phonon propagator, and $\hat{G}^{-1}(\mathbf{k}, i\omega_n) = i\omega_n\hat{\tau}_0 - \xi_{\mathbf{k}}\hat{\tau}_3 - \hat{\Sigma}(\mathbf{k}, i\omega_n)$ is the dressed electron propagator.

Migdal's theorem states that the vertex corrections to considerations given above are on the order of $\lambda_m(\Omega/E_F)$ for a momentum-independent interaction. One might therefore wonder whether the use of Migdal–Eliashberg theory is justified in FeSe/STO, since the ratio Ω/E_F is of order unity. This is bolstered by the fact that Migdal's theorem also breaks down in the limit that the small $\mathbf{q}$ scattering processes dominate. In this limit, however, one can show that the vertex corrections are still proportional to the dimensionless coupling λ_m [32]. As such, any corrections to the self-energy due to the diagrams neglected in Migdal–Eliashberg theory are of order λ^2_m, and can be treated perturbatively if the coupling is sufficiently small. As we will show, the value λ_m needed to reproduce the ARPES data is small ($\lambda_m \sim$ 0.15–0.25), indicating that we are indeed in the perturbative regime. (This is further justified by observing that the contributions to the self-energy from the second order and higher order rainbow diagrams, which are of the same order as the crossing diagrams, are small.) In this context, the work of Pietronero and coworkers is relevant [33, 34] as they have studied the contributions of the vertex corrections in the perturbative regime and found that their inclusion serves to increase the superconducting T_c when the e–ph coupling is dominated by small $\mathbf{q}$ processes. Based on these considerations, we proceed using Migdal–Eliashberg theory assuming that corrections beyond this approach can be treated at a perturbative level and will likely increase T_c further.

In what follows we parameterize the electronic dispersion as $\xi_{\mathbf{k}} = -2t[\cos(k_x a) + \cos(k_y a)] - \mu$ with $t = 75$ meV and $\mu = -235$ meV. This choice in parameters produces at Γ an electron-like Fermi pocket with $k_F = 0.97/a$ and a Fermi velocity $v_F = 0.12$ eV $\cdot a/\hbar$ along the $k_y = 0$ line, where a is the in-plane lattice constant. This closely resembles the electron pocket at M point measured by ARPES experiment. Since first principles calculations indicate that the relevant oxygen phonon branch in STO is relatively dispersionless near the Γ-point [14, 35], we approximate the phonon with a flat Einstein mode $\Omega_{\mathbf{q}} = \Omega = 100$ meV ($\hbar = 1$), which is consistent with the observed energy separation of the replica bands [7]. Furthermore, as we are interested in the case of forward scattering, we neglect any potential fermion momentum dependence in the e–ph interaction and set $g(\mathbf{q}) = g_0 \exp(-|\mathbf{q}|/q_0)$, as microscopically derived before [7, 19]. Here, q_0 sets the range of the coupling in momentum space. For different values of q_0 we adjust g_0 to obtain the desired value of the dimensionless e–ph coupling constant λ_m, which is computed from the Fermi surface averaged mass enhancement in the normal state $\lambda_m = \langle -\frac{\partial \mathrm{Re}\,\Sigma(\mathbf{k},\omega)}{\partial\omega}|_{\omega=0}\rangle$. (We are using λ_m to distinguish this definition from the standard one involving a double fermi surface average of the coupling constant $|g(\mathbf{k}, \mathbf{q})|^2$. See the supplementary material[6] for further details.) Throughout we assume an s-wave symmetry for the gap function, consistent with the observations of a

[6] For further details, please see the online supplementary material available at stacks.iop.org/njp/18/022001/mmedia.

fully gapped state on the Fermi level [1, 7, 10, 18]. Finally, we neglect the Coulomb pseudopotential μ^* in what follows. One should therefore regard our T_c values as upper bounds for the e–ph contribution to the FeSe/STO system. (Some considerations for μ^* are provided in the supplementary materials[6]. We find that its inclusion reduces T_c by $\sim$ 20% for typical values of μ^*.)

2. Analytical results

Before proceeding to full numerical solutions, we can gain some insight by first considering the case of perfect forward scattering, where the e–ph matrix element is a delta function $|g(\mathbf{q})|^2 = g_0^2 \delta_{\mathbf{q}} N$ with $g_0^2 = \lambda_m \Omega^2$ (see supplementary material[6]). In the weak coupling limit, we further set $Z(\mathbf{k}, i\omega_n) = 1$, $\chi(\mathbf{k}, i\omega_n) = 0$, and therefore $\phi(\mathbf{k}, i\omega_n) = \Delta(\mathbf{k}, i\omega_n)$. With these approximations, the gap function on the Fermi surface is given by

$$\Delta(i\omega_n) = \frac{\lambda_m \Omega^2}{\beta} \sum_m \frac{\Delta(i\omega_m)}{\omega_m^2 + \Delta^2(i\omega_m)} \frac{2\Omega}{\Omega^2 + (\omega_n - \omega_m)^2}.$$

To determine T_c we take the ansatz $\Delta(i\omega_n) = \Delta_0/[1 + (\omega_n/\Omega)^2]$ and follow the usual steps [37]: the gap equation is linearlized by setting $\Delta_0^2 = 0$ for $T \sim T_c$ and we set $\omega_{n=1}/\Omega = 0$. This results in the condition for T_c

$$1 = \frac{\lambda_m \Omega^2}{\beta_c} \sum_m \frac{2\Omega}{\omega_m^2 (1 + \omega_m^2/\Omega^2)(\Omega^2 + \omega_m^2)}.$$

The Matsubara sum can be performed exactly, yielding our final expression

$$1 = \frac{\lambda_m \beta_c}{2} \frac{2\Omega + \Omega \cosh(\Omega\beta_c) - (3/\beta_c)\sinh(\Omega\beta_c)}{1 + \cosh(\Omega\beta_c)}.$$

For the case of FeSe, $T_c \ll \Omega$, and the hyperbolic functions dominate. To the leading order, the critical temperature is *quasi-linear* in the coupling strength in the weak coupling limit, $T_c = \frac{\lambda_m}{2 + 3\lambda_m}\Omega$. (A similar result was obtained in [23] in the context of the cuprates using square-well models.) For $\lambda_m = 0.16$ and $\Omega = 100$ meV one obtains $T_c = 75$ K, which is a remarkably high temperature for such a modest value of λ_m.

The increased T_c should be compared to the standard BCS value obtained for a momentum-independent coupling. In this case, the linearized gap equation simplifies to [36, 37]

$$1 = \pi T_c \lambda_m \sum_{|\omega_m| < \Omega_D} \frac{1}{|\omega_m|} = \lambda_m \left[\ln\left(\frac{\Omega_D}{2\pi T_c}\right) - \psi\left(\frac{1}{2}\right) \right],$$

where we have expanded at large Ω_D/T_c and $\psi(z)$ is the digamma function (see supplementary material[6]). This form produces the usual exponential behavior for the critical temperature, $T_c = 1.13\Omega_D \exp(-1/\lambda_m)$, which predicts a $T_c = 2.5$ K for $\lambda_m = 0.16$ and $\Omega_D = 100$ meV.

Comparing these two results, one sees that the origin of the enhanced T_c lies in the *momentum decoupling* [24] that occurs in the Eliashberg equations when the interaction is strongly peaked at $\mathbf{q} = 0$. In the BCS case, the integration over the Fermi surface is equally weighted at all momenta, leading to a $\sum_n \frac{1}{|\omega_n|}$ term in the BCS gap equation and subsequently a leading logarithmic behavior. In the forward scattering case, there is no integration over momentum so the ω_m^{-2} term remains, resulting in a leading behavior that scales like $1/T_c$ (see supplementary material[6]). Thus, strong forward scattering serves as an ideal mechanism for producing high-T_c superconductivity [30]. Furthermore, a strong forward scattering peak in the coupling constant means that this interaction will contribute in most pairing channels [7, 23–31]. It can therefore act in conjunction with other active unconventional channels, providing another means to increase T_c further.

3. Numerical results

In real materials the e–ph interaction is expected to have a finite range q_0 in momentum space [7]. Therefore we now consider an interaction with a finite width by numerically solving the full Eliashberg equations for an e–ph coupling constant $g(\mathbf{q}) = g_0 \exp(-|\mathbf{q}|/q_0)$. Figure 1 shows the superconducting gap at the lowest Matsubara frequency $\Delta(\mathbf{k}_F, i\pi/\beta)$ as a function of temperature for several values of λ_m and $q_0 = 0.1/a$. We find that the superconducting T_c is already large for a modest value of λ_m and increases approximately linearly with λ_m in the weak coupling limit; however, the finite range of the coupling in momentum space reduces the total T_c slightly with respect to the perfect forward scattering limit (see the inset of figure 1). The linear dependence of T_c with respect to λ_m may account for the wide variation of reported T_c values in the literature, as differences in sample preparation or doping are likely to result in differences in the screening of the e–ph coupling and subsequently T_c.

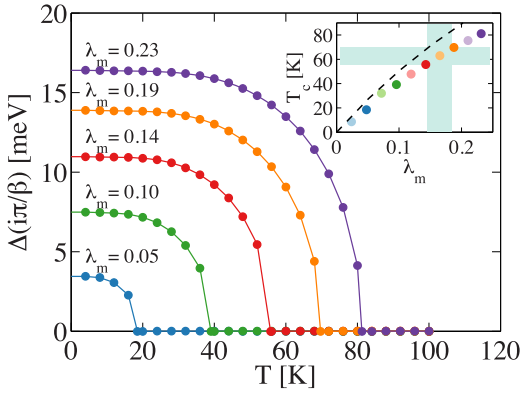

Figure 1. The superconducting gap at the smallest Matsubara frequency $\Delta(i\pi/\beta)$ as a function of temperature for various values of the e-ph coupling strength λ_m, as indicated. The e-ph coupling constant $g(\mathbf{q})$ is strongly peaked in the forward scattering direction with $q_0 = 0.1/a$. The inset shows T_c as a function of λ_m, which is extracted from the data in the main panel. The thin dashed line is the result in the limit of perfect forward scattering (see text). The shaded area represents the values of λ_m that are relevant for FeSe/STO (see supplementary material[6]).

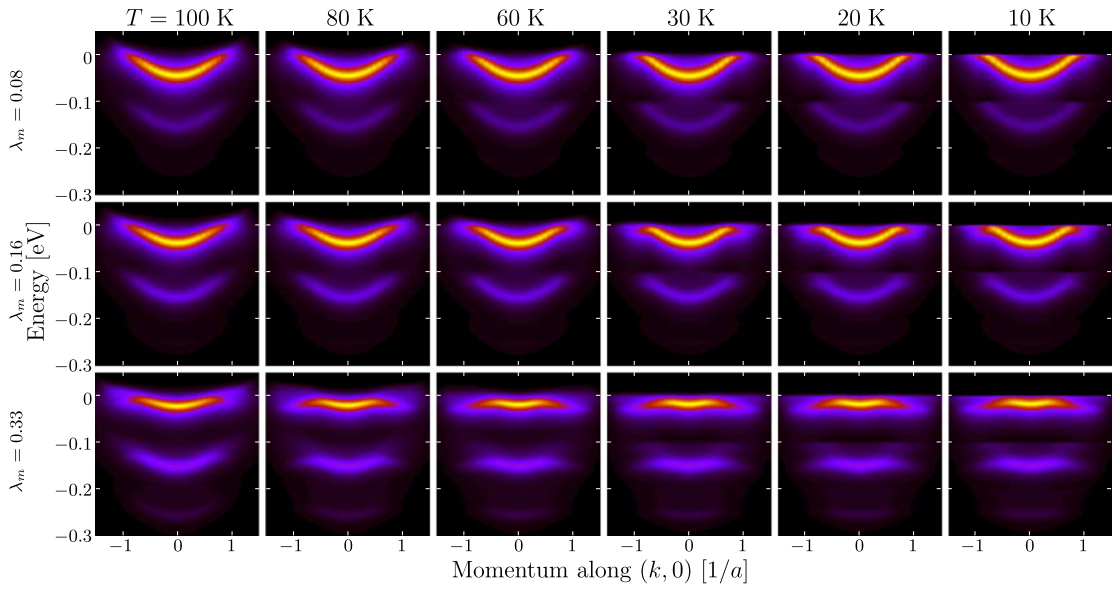

Figure 2. The temperature dependence of the spectral function for several values of the e–ph coupling λ_m.

3.1. Replica bands

The above results show that, in principle, a modest coupling to a phonon with a forward scattering peak is capable of accounting for the large T_c enhancement observed in FeSe on STO and BTO. The natural question is then how much of the experimental T_c is accounted for by this coupling? The observed shape and intensity of the replica bands [7, 8] provide us with a direct means to estimate this by comparing our model to experiment. To do so, we calculate the single particle spectral function $A(\mathbf{k}, \omega) = -\mathrm{Im}\, G_{11}(\mathbf{k}, \omega)/\pi$, which requires the analytic continuation of the self-energy to the real frequency axis using the method of [41] (see also supplementary material[6]). Figure 2 plots the temperature evolution of the spectral function obtained from a full numerical solution to our model for several values of λ_m, as indicated on the left, and $q_0 = 0.1/a$. In all cases clear replica bands are produced by the coupling, offset in energy from the main band by a fixed energy, which is Ω for small values of λ_m. The separation, however, grows for increasing λ_m. This is due to $\chi(\mathbf{k}, \omega)$, which shifts the main band upward in energy. This is most clearly seen in the $\lambda_m = 0.33$ results, where the value of k_F has visibly shrunk in the main band. In addition, for stronger values of λ_m we begin to see the formation of a second replica band located at $\sim 2\,\Omega$ below the main band. Thus the observation of only a single replica band in the bandstructure of FeSe/STO is consistent with a small λ_m.

An intuitive picture for the intensity and energy splitting of the replica band can again be obtained in the limit of perfect forward scattering. On the real axis, the zero-temperature self-consistent equation for the self-

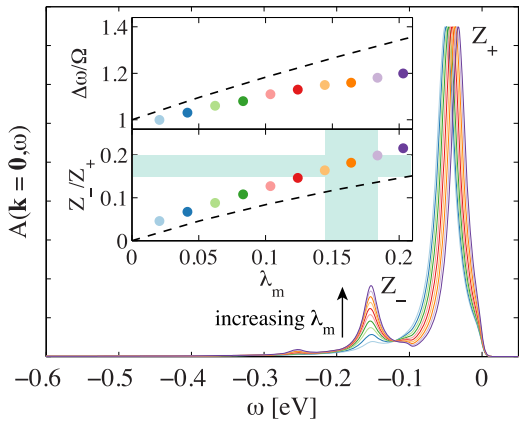

Figure 3. The spectral function for a momentum at the band bottom ($\mathbf{k} = 0$ in our model, the M point in the experiment) for $T = 30$ K, $q_0 = 0.1/a$ and $\lambda_m = 0.02 - 0.22$. The key feature of the forward scattering mechanism is the appearance of the mirror band (Z_-) next to the main band (Z_+). The relative separation $\Delta\omega$ and intensity $Z_-/Z_+ = A(0, \omega_-)/A(0, \omega_+)$ of these two features is shown in the inset, and increases approximately linearly with λ_m. The dashed lines show the corresponding result in the perfect forward scattering limit and the shaded area represents the values of λ_m that are relevant for FeSe/STO (see supplementary materials[6]).

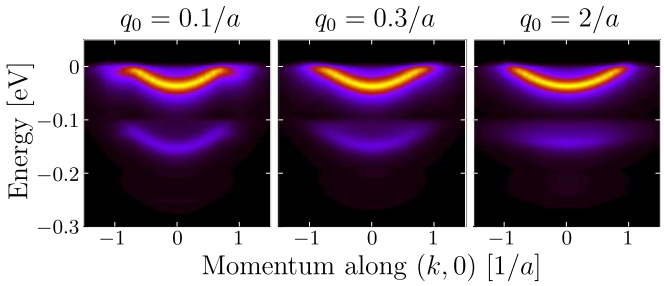

Figure 4. The spectral density $A(\mathbf{k}, \omega)$ along the $\mathbf{k} = (k/a, 0)$ cut for $q_0 = 0.1$ (left), 0.3 (middle), and 2 (right). In all three panels the temperature is $T = 30$ K and $\lambda_m = 0.14, 0.125$, and 0.25 in the left, middle, and right panels, respectively.

energy in the normal state can be written as $\Sigma(\omega) = g_0^2 G(\omega + \Omega)$. For $\xi_{\mathbf{k}} \to 0^-$, the lowest-order solution is $\Sigma(\omega) = \frac{g_0^2}{\omega + \Omega}$ (note that the $\xi_{\mathbf{k}} \neq 0$ solution can be obtained by shifting the self-energy $\Sigma(\mathbf{k}, \omega) = \Sigma(\omega - \xi_{\mathbf{k}})$). The poles of the Green's function are at $\omega = \Sigma(\omega)$, which has the solution $\omega_\pm = -\frac{\Omega}{2} \pm \frac{1}{2}\sqrt{\Omega^2 + 4g_0^2}$. The spectral weight of each pole is given by $Z_\pm = \left[1 - \frac{\partial\Sigma}{\partial\omega}\Big|_{\omega=\omega_\pm}\right]^{-1} = \left[1 + \frac{g_0^2}{(\omega_\pm + \Omega)^2}\right]^{-1}$. For small $\lambda_m = g_0^2/\Omega^2$, we find that the average energy separation between the poles is $\Delta\omega = \Omega[1 + 2\lambda_m + \mathcal{O}(\lambda_m^2)]$ and the ratio of the spectral weight is $\frac{Z_-}{Z_+} = \lambda_m + \mathcal{O}(\lambda_m^2)$, thus providing a direct measure of λ_m.

The spectral weight ratio and energy splitting between the main and replica bands can be extracted from our numerical simulations for finite values of q_0. Figure 3 shows $A(\mathbf{k}, \omega)$ for $\mathbf{k} = (0, 0)$ as a function of λ_m with $q_0 = 0.1/a$. The behavior matches our expectations gained from the perfect forward scattering limit: both the distance between the bands and the relative spectral weight grow with increasing λ_m, though the rate of increase is slower than for the case of perfect forward scattering. ARPES experiments on the FeSe/STO system [7] observe a spectral weight ratio of $\sim 0.15-0.2$ (see supplementary material[6]). Comparing to our model calculations, we extract a value of $\lambda_m \sim 0.15 - 0.2$. This corresponds to a $T_c \sim 60 - 70$ K and a gap magnitude of $\Delta \sim 10 - 15$ meV, which are consistent with measurements [1, 7, 10, 18].

In figure 4 we present the evolution of the spectral function for increasing values of q_0 where λ_m is fixed to give the same value of Z_-/Z_+. As expected, the replica bands are observed to smear both in energy and momentum as the value of q_0 is increased. This shows that a weakly momentum-dependent coupling (large q_0) to an optical mode does not reproduce the observation of a perfect replica band, with the same effective mass and

termination points in the Brillouin zone. Consequently, strong forward scattering is a necessary ingredient to understand the experimental observations [7].

4. Discussion

We have examined the consequences of an e–ph coupling that is strongly peaked in the forward scattering direction on the spectral properties and superconducting transition of a two-dimensional electronic system. We demonstrated that such a coupling produces distinct replica bands in the electronic bandstructure consistent with recent ARPES measurements on FeSe/STO and FeSe/BTO interface systems. In order to reproduce the experimentally observed spectral function, we find that relatively modest values of the e–ph coupling are needed with $\lambda_m \sim 0.15 - 0.2$. Strong forward scattering results in a momentum decoupling of the Eliashberg equations, which subsequently produces a larger superconducting T_c in comparison to the predictions of conventional BCS theory. As a result, the inferred values of λ_m predict T_c values on the order of 60–70 K due to e–ph coupling alone.

We stress that our results do not exclude the presence of another unconventional pairing channel such as spin fluctuations. The predicted values of T_c and Δ will be reduced somewhat by the inclusion of the Coulomb pseudopotential μ^*. (For example, we examined the influence of μ^* and found that T_c is lowered by $\sim$20% for $\mu^* \sim 0.2$ (see supplementary material[6]). This is much smaller than the factor of 2–5 commonly obtained for conventional phonon-mediated pairing [42, 43]. This robustness is linked to the same momentum decoupling responsible for the linear dependence of T_c on λ_m.) This reduction, however, can be overcome by the combination of the e–ph and unconventional interactions, since forward scattering will contribute to Cooper pairing in most channels [7]. An obvious way to distinguish between these possible scenarios is to measure the oxygen isotope effect. If a purely phononic mechanism is present then T_c should have an isotope coefficient $\alpha = -\partial \log(T_c)/\partial \log(M) = 1/2$, while the energy separation between the replica bands should decrease by $\sim 0.5(18 - 16)/16 \sim 6\%$ for ^{18}O rich substrates. Alternatively, in a multi-channel scenario, the isotope coefficient α will be reduced from $1/2$ when the unconventional channel is significant in comparison to the e–ph interaction [38–40]. This provides a clear means to distinguish between these scenarios.

Finally, we note that e–ph coupling with a pronounced forward scattering peak has been studied in several contexts related to of unconventional superconductivity in the cuprates [24–30] and pnictides [31]. Moreover, it is also now being addressed in the context of nematic fluctuations [44, 45]. This suggests forward scattering has a broader applicability in enhancing superconducting beyond interface systems.

Acknowledgments

We thank E Dagotto, T P Devereaux, D-H Lee, R G Moore, and J Zaanen for useful discussions. LR acknowledges funding from the Dutch Science Foundation (NWO) via a Rubicon Fellowship. TB is supported as a Wigner Fellow at the Oak Ridge National Laboratory. A portion of this research was conducted at the Center for Nanophase Materials Sciences, which is a DOE Office of Science User Facility. CPU time was provided in part by resources supported by the University of Tennessee and Oak Ridge National Laboratory Joint Institute for Computational Sciences (http://jics.utk.edu).

References

[1] Wang Q L *et al* 2012 Interface-induced high-temperature superconductivity in single unit-cell FeSe films on $SrTiO_3$ *Chin. Phys. Lett.* **29** 037402
[2] Liu D F *et al* 2012 Electronic origin of high-temperature superconductivity in single-layer FeSe superconductor *Nat. Commun.* **3** 931
[3] He S *et al* 2013 Phase diagram and electronic indication of high-temperature superconductivity at 65K in single-layer FeSe films *Nat. Mater.* **12** 605610
[4] Zhang W H *et al* 2014 Interface charge doping effects on superconductivity of single-unit-cell FeSe films on $SrTiO_3$ substrates *Phys. Rev.* B **89** 060506(R)
[5] Tan S *et al* 2013 Interface-induced superconductivity and strain-dependent spin density waves in FeSe/$SrTiO_3$ thin films *Nat. Mater.* **12** 634
[6] Zheng F, Wang Z, Kang W and Zhang P 2013 Antiferromagnetic FeSe monolayer on $SrTiO_3$: the charge doping and electric field effects *Sci. Rep.* **3** 2213
[7] Lee J J *et al* 2014 Interfacial mode coupling as the origin of the enhancement of T_c in FeSe films on $SrTiO_3$ *Nature* **515** 245
[8] Peng R *et al* 2014 Tuning the band structure and superconductivity in single-layer FeSe by interface engineering *Nat. Commun.* **5** 5044
[9] Ge J-F *et al* 2014 Superconductivity above 100K in single-layer FeSe films on doped $SrTiO_3$ *Nat. Mater.* **14** 285
[10] Peng R *et al* 2014 Measurement of an enhanced superconducting phase and a pronounced anisotropy of the energy gap of a strained FeSe single layer in FeSe/Nb:$SrTiO_3$/$KTaO_3$ heterostructures using photoemission spectroscopy *Phys. Rev. Lett.* **112** 107001
[11] Zhang W H *et al* 2014 Direct observation of high-temperature superconductivity in one-unit-cell FeSe films *Chin. Phys. Lett.* **31** 017401

[12] Liu K, Lu Z-Y and Xiang T 2012 Atomic and electronic structures of FeSe monolayer and bilayer thin films on $SrTiO_3$ (001): first-principles study *Phys. Rev.* B **85** 235123
[13] Xiang Y-Y, Wang F, Wang D, Wang Q-H and Lee D-H 2012 High-temperature superconductivity at the FeSe/$SrTiO_3$ interface *Phys. Rev.* B **86** 134508
[14] Li B, Xing Z W, Huang G Q and Xing D Y 2014 Electron–phonon coupling enhanced by the FeSe/$SrTiO_3$ interface *J. Appl. Phys.* **115** 193907
[15] Liu X *et al* 2014 Dichotomy of the electronic structure and superconductivity between single-layer and double-layer FeSe/$SrTiO_3$ films *Nat. Commun.* **5** 5047
[16] Coh S, Cohen M L and Louie S G 2015 Large electron–phonon interactions from FeSe phonons in a monolayer *New J. Phys.* **17** 073027
[17] Huang D *et al* 2015 Revealing the empty-state electronic structure of single-unit-cell FeSe/$SrTiO_3$ *Phys. Rev. Lett.* **115** 017002
[18] Fan Q *et al* 2015 Plain *s*-wave superconductivity in single-layer FeSe on $SrTiO_3$ probed by scanning tunneling microscopy *Nat. Phys.* **11** 946
[19] Lee D-H 2015 What Makes the T_c of FeSe/$SrTiO_3$ so High? *Chinese Phys.* B **24** 117405
[20] Miyata Y, Nakayama K, Sugawara K, Sato T and Takahashi T 2015 High-temperature superconductivity in potassium-coated multilayer FeSe thin films *Nat. Mater.* **14** 775
[21] Hsu F- C *et al* 2008 Superconductivity in the PbO-type structure α-FeSe *Proc. Natl Acad. Sci.* **105** 14262
[22] Li F *et al* 2015 Interface-enhanced high-temperature superconductivity in single-unit-cell $FeTe_{1-x}Se_x$ films on $SrTiO_3$ *Phys. Rev.* B **91** 220503(R)
[23] Danylenko O V, Dolgov O V, Kulić M L and Oudovenko V 1999 Normal and superconducting state in the presence of forward electron–phonon and impurity scattering *Eur. Phys. J.* B **9** 201
[24] Varelogiannis G, Perali A, Cappelluti E and Pietronero L 1996 Density-of-states-driven anisotropies induced by momentum decoupling in $Bi_2Sr_2CaCu_2O_8$ *Phys. Rev.* B **54** R6877
[25] Johnston S *et al* 2012 Evidence for the importance of extended Coulomb interactions and forward scattering in cuprate superconductors *Phys. Rev. Lett.* **108** 166404
[26] Huang Z B, Hanke W, Arrigoni E and Scalapino D J 2003 Electron–phonon vertex in the two-dimensional one-band Hubbard model *Phys. Rev.* B **68** 220507(R)
[27] Kulić M L and Zeyher R 1994 Influence of strong electron correlations on the electron–phonon coupling in high-T_c oxides *Phys. Rev.* B **49** 4395(R)
[28] Bulut N and Scalapino D J 1996 $d_{x^2y^2}$ symmetry and the pairing mechanism *Phys. Rev.* B **54** 14971
[29] Santi G, Jarlborg T, Peter M and Weger M 1996 *s*- and *d*-wave symmetries of the solutions of the Eliashberg equations *Physica* C **259** 253
[30] Kulić M L and Dolgov O V 2005 Forward scattering peak in the electronphonon interaction and impurity scattering of cuprate superconductors *Phys. Status Solidi* b **242** 151 and references therein
[31] Aperis A, Kotetes P, Varelogiannis G and Oppeneer P M 2011 Small-*q* phonon-mediated unconventional superconductivity in the iron pnictides *Phys. Rev.* B **83** 092505
[32] Wang Y, Nakatsukasa K, Rademaker L, Berlijn T and Johnston S 2016 Aspects of electron–phonon interactions with strong forward scattering in FeSe on $SrTiO_3$ substrates (arXiv:1602.00656)
[33] Pietronero L, Strassler S and Grimaldi C 1995 Nonadiabatic superconductivity: I. Vertex corrections for the electron–phonon interactions *Phys. Rev.* B **52** 10516
[34] Grimaldi C, Pietronero L and Strässler S 1995 Nonadiabatic superconductivity: II. Generalized Eliashberg equations beyond Migdal's theorem *Phys. Rev.* B **52** 10530
[35] Choudhury N, Walter E J, Kolesnikov A I and Loong C-K 2008 Large phonon band gap in $SrTiO_3$ and the vibrational signatures of ferroelectricity in $ATiO_3$ perovskites: first-principles lattice dynamics and inelastic neutron scattering *Phys. Rev.* B **77** 134111
[36] Carbotte J P 1990 Properties of boson-exchange superconductors *Rev. Mod. Phys.* **62** 1027
[37] Allen P B and Mitrović B 1982 *Solid State Physics: Advances in Research and Applications* ed H Ehrenreich *et al* vol 37 (New York: Academic) p 1
[38] Bang Y 2008 Effects of phonon interaction on pairing in high-T_c superconductors *Phys. Rev.* B **78** 075116
[39] Bang Y 2009 Isotope effect and the role of phonons in the iron-based superconductors *Phys. Rev.* B **79** 092503
[40] Johnston S, Vernay F, Moritz B, Shen Z-X, Nagaosa N, Zaanen J and Devereaux T P 2010 Systematic study of electron–phonon coupling to oxygen modes across the cuprates *Phys. Rev.* B **82** 064513
[41] Marsiglio F, Schossmann M and Carbotte J P 1988 Iterative analytic continuation of the electron self-energy to the real axis *Phys. Rev.* B **37** 4965
[42] Sanna A, Pittalis S, Dewhurst J K, Monni M, Sharma S, Ummarino G, Massidda S and Gross E K U 2012 Phononic self-energy effects and superconductivity in CaC_6 *Phys. Rev.* B **85** 184514
[43] Margine E R and Giustion F 2014 Two-gap superconductivity in heavily *n*-doped graphene: ab initio Migdal–Eliashberg theory *Phys. Rev.* B **90** 014518
[44] Lederer S, Schattner Y, Berg E and Kivelson S A 2015 Enhancement of Superconductivity near a nematic quantum critical point *Phys. Rev. Lett.* **114** 097001
[45] Maier T A and Scalapino D J 2014 Pairing interaction near a nematic quantum critical point of a three-band CuO_2 model *Phys. Rev.* B **90** 174510